ChemComm

ROYAL SOCIETY OF CHEMISTRY

COMMUNICATION

View Article Online
View Journal | View Issue

Cite this: *Chem. Commun.*, 2026, **62**, 2917

Received 27th August 2025,
Accepted 19th December 2025

DOI: 10.1039/d5cc04918k

rsc.li/chemcomm

Hollow polydopamine spheres decorated with MoS_2 nanosheets for the hydrogen evolution reaction

Raphaella T. S. Gonçalves, [ab] Matheus F. F. das Neves, [c] Carlos Ospina[c] and Murilo Santhiago *[ac]

Hollow carbon spheres decorated with MoS_2 (HCS@MoS_2) were synthesized using SiO_2 templating and polydopamine carbonization. The porous carbon shell enlarges the electrochemically active surface area, while flower-like mixed-phase MoS_2 nanosheets expose catalytic sites. The ecofriendly electrocatalyst exhibits a low HER overpotential (0.3 V at 10 mA cm^{-2}) and remarkable stability.

Hollow carbon spheres (HCSs) are structures composed of a carbon shell and internal voids that confer on them unique features, such as high surface area, low specific density, tunable porosity, mechanical strength, and thermal and chemical stability.[1] HCSs can be mainly synthesized by the three methods: hard templating, soft templating and self-assembly. Among them, hard templating using SiO_2 or polystyrene spherical particles coated with carbon shell precursors is the most employed method due to the possibility to control the thickness of HCSs after annealing. These structures have been employed in several applications in the energy field, for instance, lithium batteries,[2] sodium-ion batteries,[3] and supercapacitors.[4–6] Hydrogen is an important clean source of energy that can be obtained by electrochemical water splitting where the hydrogen evolution reaction (HER) takes place in one of the electrodes. However, HCSs have been mainly functionalized with scarce and expensive materials such as Pt[7] and Rh,[8] thus demanding low-cost, abundant, non-toxic, and stable electrocatalysts.

Transition metal dichalcogenides consist of relatively cheap transition metals and earth-abundant chalcogen elements and have shown enormous potential to replace noble metals in the HER due to their remarkable physical and chemical properties.[9–11] Particularly, molybdenum disulfide (MoS_2) has many of the advantages mentioned above; however, the pristine three-atom thick monolayer contains catalytic sites only at the edges of the nanosheets.[12] Thus, one of the unmet challenges is engineering MoS_2 nanosheets on the surface of HCSs to expose the catalytic sites to drive the HER using mild conditions. A few attempts to engineer MoS_2 nanosheets on the shell of HCSs focused on multiple chemical precursors and harmful chemicals, such as the presence of resorcinol-formaldehyde,[5] which contains two toxic components, thus limiting the preparation of simple and eco-friendly functionalized electrodes for the HER.

Herein, in this work, we report for the first time the use of polydopamine (PDA) to chemically engineer the nano-building blocks with MoS_2 nanosheets for the HER. The MoS_2 nanosheets were grown on HCSs using a simple hydrothermal method. The hollow structure with MoS_2 nanosheets avoids the restacking of MoS_2 and improves the electron transfer and diffusion from the outer shell to the inner shell and *vice versa* during electrocatalysis. The ultra-thin functional layer was characterized by transmission electron microscopy (TEM) and X-ray photoelectron spectroscopy (XPS), among other techniques. The functional nanolayer is approximately 50 nm thick and shows the presence of the 1T MoS_2 phase, thus contributing to the electrocatalytic process. Electrochemical assays exhibit a low overpotential of 300 mV and a Tafel slope of 167 mV dec^{-1} in 0.5 M H_2SO_4 electrolyte solution. The HCS@MoS_2 electrodes are stable and present high electrochemically active surface area when compared to pristine MoS_2 electrodes. Materials, synthesis of HCS and HCS@MoS_2, preparation of the electrodes and characterization techniques are available in the SI, and the chemical synthesis of HCS@MoS_2 is concisely illustrated in Fig. 1a.

Initially, SiO_2 nanoparticles were synthesized using the Stöber method. These nanoparticles are spherical with an average diameter of 330 nm, as depicted in Fig. 1b and Fig. S1. Next, the SiO_2 nanoparticles were coated with PDA resulting in a texturized surface, as illustrated in Fig. 1c. PDA is

[a] *Postgraduate Program in Nanosciences and Advanced Materials. Federal University of ABC, Santo André, São Paulo 09210-580, Brazil, murilo.santhiago@lnnano.cnpem.br*
[b] *Ilum School of Science, Brazilian Center for Research in Energy and Materials, Campinas, São Paulo 13083-970, Brazil*
[c] *Brazilian Nanotechnology National Laboratory, Brazilian Center for Research in Energy and Materials, Campinas, São Paulo 13083-970, Brazil*

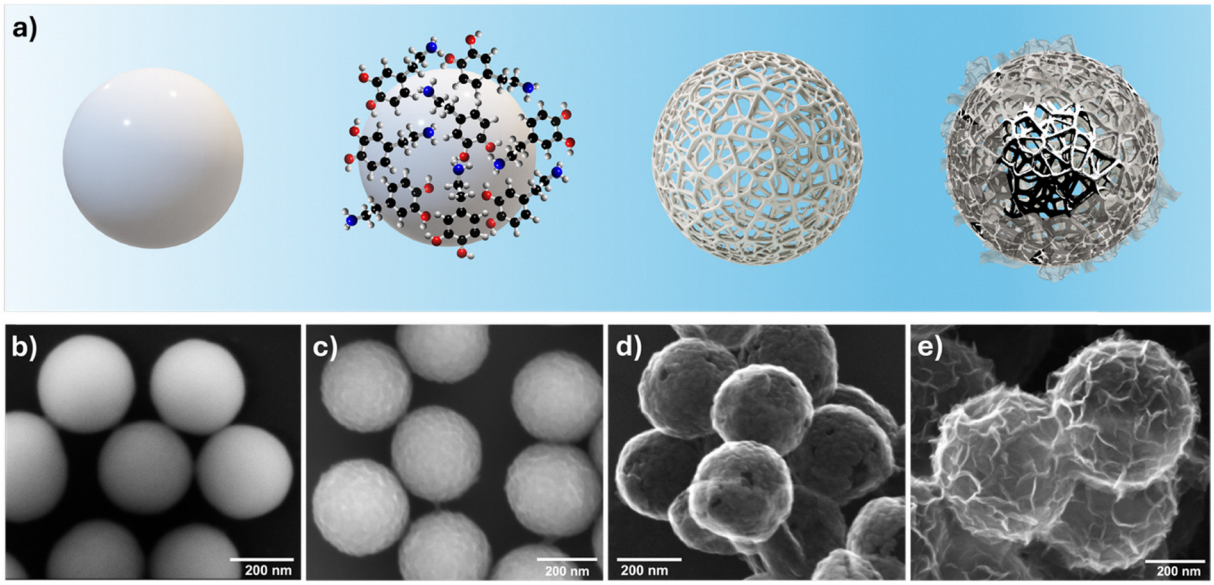

Fig. 1 (a) Scheme of the preparation of HCS@MoS_2. (b) SEM images of the SiO_2 nanoparticles, (c) SiO_2 functionalized with PDA, (d) HCS and (e) HCS@MoS_2.

a biomimetic, non-toxic, biocompatible and self-adherent polymer, which can be easily deposited on a wide variety of materials by the self-polymerization of dopamine at room temperature in aqueous solutions.[13]

The thickness of PDA can be tuned by controlling the polymerization time, as reported.[14] However, thin films of PDA are mechanically weak, and it is recommended to conduct the functionalization for at least 24 h or repeat the coating process. DLS analysis, shown in Fig. S2, revealed a hydrodynamic diameter of ~507 nm for PDA-coated SiO_2 nanoparticles, compared to ~407 nm for bare SiO_2, indicating a PDA layer of ~100 nm. As DLS accounts for the solvation layer and interfacial interactions in aqueous media, these values exceed the physical sizes observed by SEM. The ~65 nm difference between DLS and SEM for bare SiO_2 highlights the influence of the hydration shell on DLS measurements. By removing the core using NaOH, one can observe the formation of HCSs, as illustrated in Fig. 1d. In the last step, Fig. 1e, the MoS_2 nanosheets were synthesized by combining Mo and S precursors. The nanoparticles were homogeneously covered by the MoS_2 nanosheets.

Preserving the morphology during the PDA processing is essential when preparing hollow materials like carbon spheres. Thermal annealing significantly enhances the mechanical properties of PDA attached to substrates, although it also reduces the thickness due to mass loss. For instance, when annealed at 1000 °C, PDA is converted into a conductive material suitable for electrochemical applications. Such higher temperatures are not appropriate for free-standing and thin films, *i.e.* HCSs, due to high mass loss, as shown in Fig. S3. Thus, PDA was thermally treated at 400 °C to improve the mechanical properties of the nanoparticles. The hollow nature of the nanoparticles and the thickness after the thermal treatment can be observed in the TEM images illustrated in Fig. 2a and c. The thickness of PDA is reduced by approximately 70%, resulting in a carbon shell of 32 nm. In addition, the diffraction pattern in Fig. 2d reveals that HCSs are amorphous. Raman spectroscopy was also performed to evaluate the carbon shell. The spectrum exhibits the characteristic D and G bands of graphitic carbon,[15] confirming the successful carbonization of the polydopamine layer. The corresponding Raman spectrum is provided in the SI (Fig. S4). Fig. 2a–d shows the TEM images of the HCS, and Fig. 2e–h shows the TEM images of the HCS@MoS_2. As can be observed, the spherical morphology is preserved, and MoS_2 nanosheets are clearly observed decorating the HCS. Fig. S5(a and b) highlights the crystalline fringes of the MoS_2 nanosheets, and the corresponding fast Fourier transform (FFT) pattern further confirms their lattice periodicity. The chemical composition of HCS@MoS_2 was further confirmed using energy-dispersive X-ray spectroscopy (EDX) analysis. The scanning TEM (STEM) image and the respective elemental maps are shown in Fig. 2i and j–o, respectively. Mo and S are visible in the maps homogeneously distributed over the shell of the nanoparticles. EDX analysis displays the signals of Mo and S, not distinguishing them individually, but rather confirming their co-localization. This is due to the overlap between the Mo Lα (~2.29 keV) and S Kα (~2.30 keV) peaks, which prevents precise separation but provides evidence that both elements co-localize in the same regions, thus confirming the presence of MoS_2. The detection of the chemical elements C, N, and O confirms the presence of polydopamine. Note that the permanence of N and O is because the nanoparticles were not treated at high temperatures. The retention of these elements helps to make the surface more hydrophilic and consequently facilitates the diffusion of hydronium ions into the surface of the electrocatalyst.

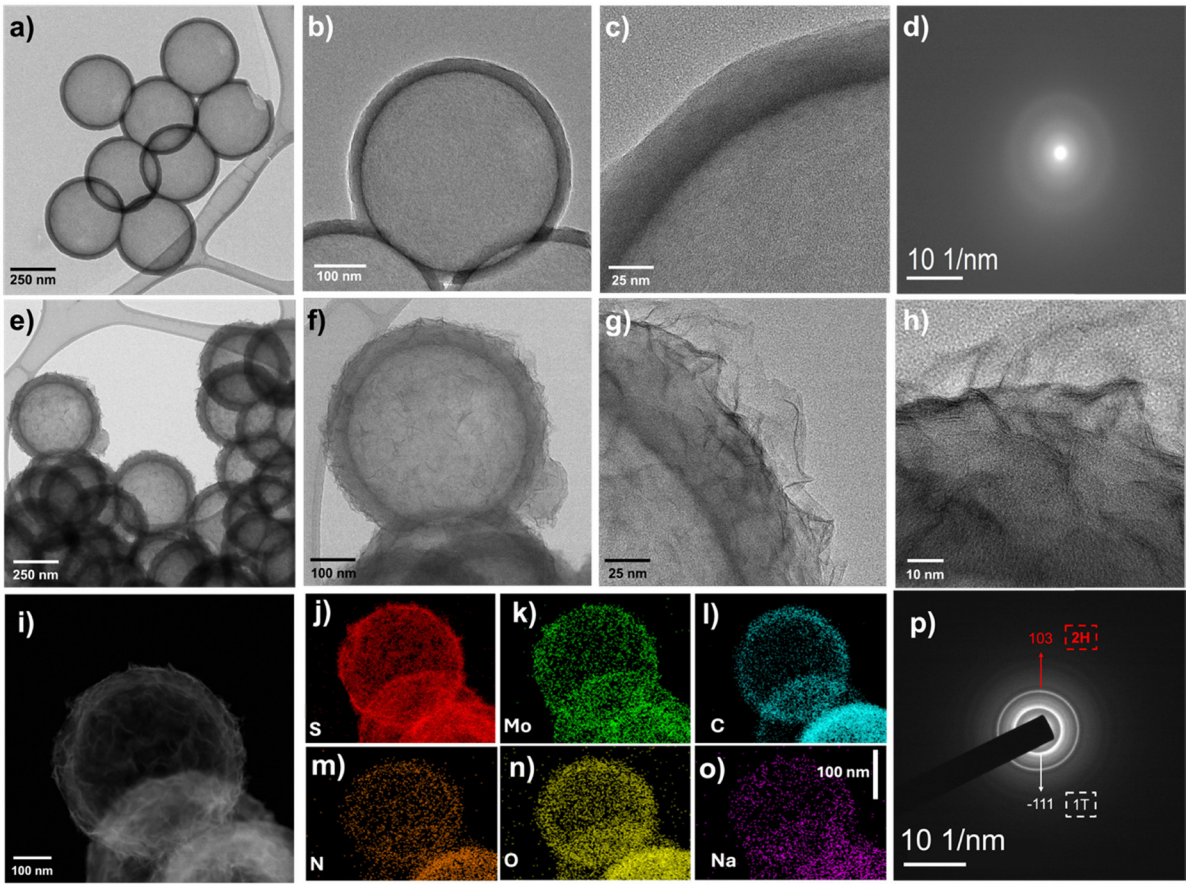

Fig. 2 (a)–(c) TEM images of the HCS at different magnifications. (d) Electron diffraction pattern of the HCS. (e)–(h) TEM images of the HCS@MoS_2 at different magnifications. High-angle annular dark-field scanning TEM (HAADF-STEM) image of the (i) HCS@MoS_2 and the respective elemental maps for (j) S, (k) Mo, (l) C, (m) N, (n) O and (o) Na by energy-dispersive X-ray spectroscopy (EDS). (p) Electron diffraction pattern of the HCS@MoS_2.

In addition, the hollow architecture observed in the TEM images inherently provides an accessible pore structure that facilitates electrolyte penetration throughout the carbon shell, further contributing to the increased electrochemical surface accessibility of the material. Additional SEM images (Fig. S6) provide a detailed view of the surface pores in the carbon shell. Furthermore, such nitrogen-containing species derived from PDA are known to modulate surface wettability and interfacial electronic properties.[16] Finally, sodium was also found in the shell due to the use of sodium molybdate and the Mo precursor in the synthesis.

The diffraction analysis of the MoS_2 nanosheets obtained by the chemical route shown in Fig. 2p revealed two diffraction rings belonging to the reflections of the (103) and (−111) planes of the hexagonal and tetragonal phases of MoS_2, respectively, thus showing the mixture of crystalline 2H and 1T phases of MoS_2.[5]

It is well known that the catalytic active sites of pristine MoS_2 are located at edges rather than on the basal plane. Interestingly, the TEM images revealed that the nanosheets are edge-oriented and consequently expose the catalytic sites to the electrolyte. In addition, many synthesized MoS_2 present vacancies and defects due to the incomplete formation of chemical bonds on the basal plane.[17–19] This scenario is relevant for the HER because it increases the number of catalytic sites on the basal plane. From XPS analysis, the S/Mo ratio was found to be 3.7, indicating that the synthesized material contains excess sulphur which helps to promote the HER process.[20] The high-resolution spectra of molybdenum and sulphur are shown in Fig. S7a and b. The peaks of Mo^{4+} $3d_{5/2}$, Mo^{4+} $3d_{3/2}$, and Mo^{6+} $3d_{3/2}$ can be observed at 230.1, 233.3, and 235.3 eV, respectively. In the S region, S $2p_{3/2}$ and S $2p_{1/2}$ peaks are found at 163.0 and 164.1 eV, respectively.[12,21] Additionally, in the Mo spectra small peaks shifting (~1 eV) to smaller binding energies is observed, which clearly indicates the presence of the 1T phase as reported.[21–24] The fraction between areas indicates that 2H:1T is around 0.7. Additional peaks were also observed in the S region, thus confirming the presence of a mixed phase. Additionally, the peaks observed in the region around 168 eV indicate oxidized S atoms.[25] Additional information is found in the SI. The high-resolution spectra are shown in Fig. S7, which confirm the presence of a mixed MoS_2 phase, in agreement with previous studies.[21,23] It is important to mention that the majority of the tetragonal phase enhances the electrical conductivity besides helping to drive the HER.[26]

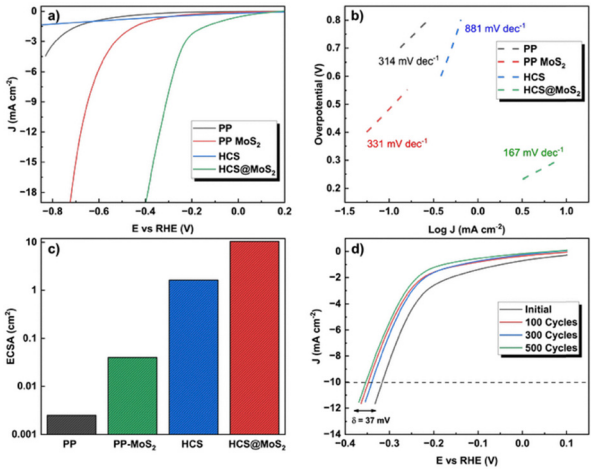

Fig. 3 (a) HER polarization curves for PP, HCS, MoS_2 control and HCS@MoS_2 in 0.5 M H_2SO_4 solution at 5 mV s^{-1}. (b) Tafel plots for the investigated materials. (c) ECSA. (d) Stability test.

The electrocatalytic performance of HCS@MoS_2 and control samples for the HER was studied using pyrolyzed carbon electrodes. The nanoparticles loaded on the PP electrodes are attached between fibers and pores, as shown in Fig. S8. Full characterization data have already been reported in the literature.[27] Linear sweep voltammetry in 0.5 M H_2SO_4 solution purged with N_2 using a three-electrode setup showed high overpotentials for both carbon electrodes and HCSs due to insufficient active sites for the HER (Fig. 3a). Conversely, HCS@MoS_2 had significantly lower overpotential at 10 mA cm^{-2}, even compared to pristine MoS_2, corresponding to 300 mV for HCS@MoS_2 against 665 mV for control MoS_2 on PP. The control samples contain only the naturally occurring edges as active sites. Representative HER benchmarks for Pt/C and recent state-of-the-art MoS_2-based catalysts are shown in Table S1. Tafel plots from the voltammetry curves (Fig. 3b) revealed that HCS@MoS_2 had a much lower Tafel slope of 167 mV dec^{-1}, corroborating the higher HER activity. The electrochemically active surface area (ECSA) was calculated from the cyclic voltammograms obtained at different scan rates. The plot of $\Delta I/2$ *versus* scan rate yielded the double-layer capacitance, as shown in Fig. S9. Fig. 3c displays the ECSA results, indicating that HCS@MoS_2 has a higher ECSA due to the nanostructured HCS particles with defective MoS_2 nanosheets, up to 250 times higher than that of PP-MoS_2.

The porous nature of the nanoparticles allows the hydronium ions to diffuse through the functional shell. Successive cyclic voltammetric curves were obtained to assess the electrochemical stability of HCS@MoS_2, with results showing that the nanomaterials withstand up to 500 cycles, as shown in Fig. 3d, thus highlighting the remarkable stability of the nanoparticles. Furthermore, post-cycling microscopy (Fig. S10a and b) demonstrates that neither the carbon shell nor the MoS_2 nanosheets undergo morphological degradation after 500 cycles. In addition, post-cycling XPS analysis (Fig. S11) confirms that the MoS_2 framework is partially oxidized after the stability test.

In conclusion, we engineered hollow carbon spheres coated with polydopamine and decorated with MoS_2 nanosheets for HER applications. Mechanically stable HCSs with thin carbon layers were obtained, and hydrothermal synthesis yielded sulphur-rich mixed-phase MoS_2. The porous carbon framework enhanced the electrochemically active surface area, favouring electrocatalysis. As a result, HCS@MoS_2 exhibited low overpotential and remarkable cycling stability.

The manuscript was written through the contributions of all authors. All authors have given approval to the final version of the manuscript.

Conflicts of interest

There are no conflicts to declare.

Data availability

All data obtained will be stored on the researcher's personal computer, in cloud services (One Drive) and in the repository of the Brazilian Center for Research in Energy and Materials (CNPEM). Files saved in the three locations described above will be organized as follows: technique > measurement date > sample > experimental conditions, to facilitate quick location. Records noted as sample preparation and experimental conditions will be made in a laboratory notebook that belongs to the research center, which will be available for internal and external consultation.

Additional data were also provided in the supplementary information (SI) file. Supplementary information is available. See DOI: https://doi.org/10.1039/d5cc04918k.

Acknowledgements

This research used facilities of the Brazilian Nanotechnology National Laboratory (LNNano), part of the Brazilian Center for Research in Energy and Materials (CNPEM), a private non-profit organization under the supervision of the Brazilian Ministry for Science, Technology, and Innovations (MCTI). The transmission electron microscopy staff are acknowledged for the assistance during the experiments (Proposal ILUM-3-20242375). The authors also thank ILUM – School of Science. Financial support was provided by the São Paulo Research Foundation (FAPESP) through CEMol (CEPID Grant No. 2024/00989-7). M.S. acknowledges FAPESP (Grants 2024/15173-2, 2023/17576-4, 2024/18470-8) and CNPq (405011/2025-3, 304999/2025-3) and M.F.F.N. acknowledges FAPESP for their post-doctoral fellowship (Grant No. 2023/15689-6).

References

1 T. Liu, L. Zhang, B. Cheng and J. Yu, *Adv. Energy Mater.*, 2019, **9**, 1803900.
2 Y. Feng, J. Xi, Z. Lin, Z. Lin, W. W. Yan, Y. Yuan and S. Guo, *ACS Appl. Nano Mater.*, 2024, **7**, 22534–22544.
3 R. Liu, B. Zhang, L. Fu, Z. Fu, H. Xie, Y. Tang, H. Wang and D. Sun, *Mater. Today Chem.*, 2024, **35**, 101903.

4 W. Liu, M. Zhu, J. Liu, W. Hu, X. Li and J. Liu, *Inorg. Chem. Front.*, 2018, **5**, 2198–2204.
5 C. Liu, P. Yang and X. Zhang, *Int. J. Hydrogen Energy*, 2025, **97**, 1348–1356.
6 J. Du, Q. Han, Y. Chen, M. Peng, L. Xie and A. Chen, *Angew. Chem., Int. Ed.*, 2024, **63**, e202411066.
7 V. Verma, S. R. Choudhury, V. Rathour, S. R. Choudhury and V. Ganesan, *Microporous Mesoporous Mater.*, 2024, **367**, 113005.
8 Y. Wang, Z. Chen, C. Zhang, L. Yang, Q. Jiang, J. Zhang, H. He and H. Huang, *Inorg. Chem.*, 2024, **63**, 16888–16896.
9 Y. Shen, S. He, Y. Zhuang, S. Huang, C. Meng, A. Yuan, W. Miao and H. Zhou, *ACS Appl. Nano Mater.*, 2023, **6**, 16873–16881.
10 S. Qiang, J. Chen, S. Huang, H. Xu, X. Zhuo, H. Zhou, A. Yuan, H. Zhou and Y. Qiao, *J. Colloid Interface Sci.*, 2026, **701**, 138722.
11 Q. Deng, Z. Li, R. Huang, P. Li, H. Gomaa, S. Wu, C. An and N. Hu, *J. Mater. Chem. A*, 2023, **11**, 24434–24453.
12 C. De Lourenço, A. B. S. De Araújo, L. H. Hasimoto, I. A. A. Feitosa, M. F. F. Das Neves, J. Bettini, T. M. Perfecto, T. C. R. Rocha, T. J. A. Mori, E. R. Leite and M. Santhiago, *J. Mater. Chem. A*, 2025, **13**, 951–960.
13 H. Lee, S. M. Dellatore, W. M. Miller and P. B. Messersmith, *Science*, 2007, **318**, 426–430.
14 J. F. Rocha, J. C. De Oliveira, J. Bettini, M. Strauss, G. S. Selmi, A. K. Okazaki, R. F. De Oliveira, R. S. Lima and M. Santhiago, *ACS Meas. Sci. Au*, 2024, **4**, 188–200.
15 J. F. Rocha, J. C. De Oliveira, J. Bettini, M. Strauss, G. S. Selmi, A. K. Okazaki, R. F. De Oliveira, R. S. Lima and M. Santhiago, *ACS Meas. Sci. Au*, 2024, **4**, 188–200.
16 Q. Yang, Z. Wang, L. Dong, W. Zhao, Y. Jin, L. Fang, B. Hu and M. Dong, *J. Phys. Chem. C*, 2019, **123**, 10917–10925.
17 Y. Liu, S. Guan, X. Du, Y. Chen, Y. Yang, K. Chen, Z. Zheng, X. Wang, X. Shen, C. Hu and X. Li, *Energy Fuels*, 2023, **37**, 5370–5377.
18 J. Wang, Z. Sun, Y. Li, L. Guo, Y. Wang, C. Fan, Y. Wang, R. Li, X. Zhang, F. Li, Z. Yu and J. Liu, *J. Alloys Compd.*, 2023, **955**, 170199.
19 J. Radhakrishnan, A. Kareem, S. Senthilkumar and K. Biswas, *J. Alloys Compd.*, 2022, **917**, 165444.
20 B. R. Florindo, L. H. Hasimoto, N. De Freitas, G. Candiotto, E. N. Lima, C. De Lourenço, A. B. S. De Araujo, C. Ospina, J. Bettini, E. R. Leite, R. S. Lima, A. Fazzio, R. B. Capaz and M. Santhiago, *J. Mater. Chem. A*, 2023, **11**, 19890–19899.
21 A. D. Marinov, L. Bravo Priegue, A. R. Shah, T. S. Miller, C. A. Howard, G. Hinds, P. R. Shearing, P. L. Cullen and D. J. L. Brett, *ACS Nano*, 2023, **17**, 5163–5186.
22 C. A. Papageorgopoulos and W. Jaegermann, *Surf. Sci.*, 1995, **338**, 83–93.
23 G. Eda, H. Yamaguchi, D. Voiry, T. Fujita, M. Chen and M. Chhowalla, *Nano Lett.*, 2011, **11**, 5111–5116.
24 M. Ozhukil Valappil, T. Siu, B. Y. Martin, N. D. Wilson, V. Rajakumaran, D. Kanani, J. Konieczny, J. J. Medvedev, J. Ouyang, N. Graddage, R. D. L. Smith, F. Münzer and M. A. Pope, *Chem. Mater.*, 2025, **37**, 5658–5671.
25 S. Venkateshwaran, A. Ajith, V. Duraisamy, A. Krishnan and S. M. Senthil Kumar, *Inorg. Chem.*, 2023, **62**, 841–852.
26 W. Liu, S. Zhu, M. Ran, Z. Fu, M. Zhang, Y. Zhang, H. Wang, M. Xing and P. Fu, *Angew. Chem., Int. Ed.*, 2025, e202504749.
27 L. H. Hasimoto, J. Bettini, E. R. Leite, R. S. Lima, J. B. Souza Junior, L. Liu and M. Santhiago, *ACS Appl. Eng. Mater.*, 2023, **1**, 708–719.